Vortex charging effect in a chiral $p_x \pm ip_y$-wave superconductor

Masashige Matsumoto[1] and Rolf Heeb[2]
[1]*Department of Physics, Faculty of Science, Shizuoka University, 836 Oya, Shizuoka 422-8529, Japan*
[2]*Theoretische Physik, Eidgenössische Technische Hochschule Hönggerberg, CH-8093 Zürich, Switzerland*
(Received 24 August 2001; published 29 November 2001)

Quasiparticle states around a single vortex in a $p_x \pm ip_y$-wave superconductor are studied on the basis of the Bogoliubov–de Gennes (BdG) theory, where both charge and current screenings are taken into account. Due to the violation of time-reversal symmetry, there are two types of vortices which are distinguished by their winding orientations relative to the angular momentum of the chiral Cooper pair. The BdG solution shows that the charges of the two types of vortices are quite different, reflecting the rotating Cooper pair of the $p_x \pm ip_y$-wave paring state.

DOI: 10.1103/PhysRevB.65.014504 PACS number(s): 74.60.Ec, 71.27.+a, 74.25.Jb, 74.60.Ge

I. INTRODUCTION

The discovery of many types of superconductors from heavy fermion compounds to high-T_c cuprates has driven us to study a large variety of new physics beyond the standard BCS theory for conventional *s*-wave superconductors. The study of the unconventional superconductivity was stimulated by the discovery of superfluid ^{3}He in which a spin triplet *p*-wave state is realized. Unlike the conventional *s*-wave state, the *p*-wave state has both spin and orbital degrees of freedom. This is the most pronounced feature of the unconventional superconductors, observed in their thermodynamics and impurity effects or detected by tunneling spectroscopy, nuclear magnetic resonance (NMR), muon spin relaxation (μSR) measurements, and so on.

Sr_2RuO_4 is the first layered perovskite compound showing superconductivity without CuO_2 planes.[1] Recent experimental and theoretical studies indicated that the superconducting pairing symmetry of Sr_2RuO_4 is not a simple *s*-wave. The absence of a Hebel-Slichter peak in nuclear quadrupole resonance (NQR),[2] and the sensitivity of T_c on nonmagnetic impurities,[3] pointed toward an unconventional pairing. The indication of broken time reversal symmetry,[4] observed in μSR measurements, gives a strong argument for the unconventional paring state. A Knight shift experiment showed that spin susceptibility is not affected by the superconducting state,[5] which is strong evidence of a spin-triplet pairing. Sigrist *et al.* suggested that a $p_x \pm ip_y$-wave state, which breaks the time-reversal symmetry in a tetragonal crystal field, is the most likely pairing state for Sr_2RuO_4.[6] The line node behavior reported in the latest experiments[7–9] is related to low-temperature thermodynamical measurements, such as specific heat and NMR T_1^{-1}. An orbital-dependent superconductivity[10] and gap anisotropy[11,12] were suggested to understand the line node behavior. Here we focus on the $p_x \pm ip_y$-wave pairing state, since this representation is the simplest and essential form. We will see a rich physics of this chiral state.

The most intriguing character of the $p_x \pm ip_y$-wave state is that the Cooper pair has a ± 1 angular momentum, i.e., the pair electrons are rotating. This property is similar to that of the *A* phase of the superfluid ^{3}He. Due to the violation of the time-reversal symmetry, we have two types of vortices, one of which is in the same direction to the angular momentum of the rotating Cooper pair, and the other is in the opposite direction. The rotating pair shows up in quasiparticle states around a vortex core.

In this paper we present an interesting physics related to a vortex. We focus on a vortex charging effect.[13] It was pointed out that for an *s*-wave superconductor the vortex charge is proportional to the slope of the density of states at the Fermi level.[14] Hayashi *et al.* proposed that the vortex charge is determined by the quasiparticle structure in the vortex core[15] rather than the slope of the density of states. Very recently, it was reported that Chern-Simons terms lead to a fractional vortex charge for the $p_x \pm ip_y$-wave state.[16] Thus the origin of the vortex charge is still controversial. To make this point clearer, we investigate the vortex charging effect in a chiral $p_x \pm ip_y$-wave state, concentrating our attention on the microscopic origin of the vortex charge. This is demonstrated by solving the Bogoliubov-de Gennes (BdG) equation self-consistently, including both charge and current screenings. To our knowledge, this is the first fully self-consistent BdG study of a single vortex. We would like to show how the rotating Cooper pair shows up in the vortex charging effect.

This paper is organized as follows. In Sec. II, we present our formulation for calculating quasiparticle states near the vortex core based on the BdG equation. In Sec. III, we show numerical results. We give a summary and discussions in Sec. IV.

II. FORMULATION

Let us begin with the following BdG and gap equations for the $p_x \pm ip_y$-wave state:[17–19]

$$h_0 u_n - \frac{i}{k_F} \sum_{\pm} \left[\Delta_{\pm} \Box_{\pm} + \frac{1}{2} (\Box_{\pm} \Delta_{\pm}) \right] v_n = E_n u_n, \quad \text{(1a)}$$

$$-h_0^* v_n - \frac{i}{k_F} \sum_{\pm} \left[\Delta_{\pm} \Box_{\pm} + \frac{1}{2} (\Box_{\pm} \Delta_{\pm}) \right]^* u_n = E_n v_n, \quad \text{(1b)}$$

$$h_0=\frac{1}{2m}\left(-i\nabla+\frac{e}{c}\boldsymbol{A}\right)^2-eA_0-\mu, \tag{1c}$$

$$\Delta_{\pm}(\boldsymbol{r})=-i\frac{V_p\Omega}{2k_F}\sum_{0\leqslant E_n\leqslant E_c}\tanh\left(\frac{E_n}{2T}\right)[v_n^*(\boldsymbol{r})\Box_{\mp}u_n(\boldsymbol{r})-u_n(\boldsymbol{r})\Box_{\mp}v_n^*(\boldsymbol{r})]. \tag{1d}$$

A detailed derivation is given in the Appendix. Throughout this paper, we use $\hbar=1$ and $k_B=1$ units. $e>0$ is the electron charge. E_n is the energy eigenvalue for the superconducting quasiparticle, and $\Box_{\pm}=\partial_x\pm i\partial_y$ is used. A_0 and $\boldsymbol{A}$ are the scalar and vector potentials, respectively. $V_p>0$ and Ω are the p-wave attractive interaction and the volume of the two-dimensional system, respectively. E_c is a cutoff energy, and μ is a chemical potential. $\Delta_{\pm}$ is the order parameter for the $p_x\pm ip_y$-wave. For simplicity, we assume that the superconductor is basically two dimensional, and has a cylindrical Fermi surface. We note that the BdG solution has the following time-reversal relation:

$$\{u_{-E_n},v_{-E_n}\}=\{v_{E_n}^*,u_{E_n}^*\}. \tag{2}$$

The solution of the BdG equation determines the two-dimensional electron and current densities:

$$n(\boldsymbol{r})=2\sum_{E_n}|u_n(\boldsymbol{r})|^2f(E_n), \tag{3a}$$

$$\boldsymbol{J}(\boldsymbol{r})=-\frac{ie}{m}\sum_{E_n}[u_n^*(\boldsymbol{r})\nabla u_n(\boldsymbol{r})-u_n(\boldsymbol{r})\nabla u_n^*(\boldsymbol{r})]f(E_n)-\frac{e^2}{mc}n(\boldsymbol{r})\boldsymbol{A}(\boldsymbol{r}). \tag{3b}$$

By using relation (2), both densities have been expressed in terms of the u_n amplitude. $f(E_n)$ is the Fermi distribution function, and the E_n summation in Eq. (3) runs both negative and positive regions. The scalar and vector potentials obey the Maxwell equations

$$\nabla^2A_0(\boldsymbol{r})=-\frac{4\pi e}{d}[n_0-n(\boldsymbol{r})], \tag{4a}$$

$$\nabla^2\boldsymbol{A}(\boldsymbol{r})=-\frac{4\pi}{cd}\boldsymbol{J}(\boldsymbol{r}). \tag{4b}$$

We have introduced a layer spacing d to convert the area densities into volume densities. To satisfy charge neutrality we introduce a uniform n_0 as the density of positive background charge. We have taken the origin of the coordinate at the vortex center.

In the bulk region p_x+ip_y and p_x-ip_y-wave states are degenerate. In this paper we will choose one of the two degenerate states, the p_x+ip_y-wave state, as a dominant component. However, the other component (p_x-ip_y) is admixed with the bulk state (p_x+ip_y) close to the vortex core.[20] Therefore, our formulation includes both $p_x\pm ip_y$ components. The p_x+ip_y-wave state has a $+1$ Cooper pair phase winding, since $\Box_+$ in Eq. (1) is expressed as

$$\Box_+=e^{i\phi}\left(\partial_r+\frac{i}{r}\partial_\phi\right). \tag{5}$$

Here r and ϕ are the two-dimensional polar coordinates. A single vortex produces an additional phase winding of ±1. Therefore, there are two kind of vortices: the vortex winding direction is parallel or antiparallel relative to the Cooper pair winding. As we will see later, the former vortex is charged up, while the latter is not. We call the former and the latter a C (charged) vortex and a U (uncharged) vortex, respectively. The C vortex has an effective twofold winding of $+2$. On the other hand, the phase winding is zero for the U vortex, since the winding of the Cooper pair cancels the vortex pair. Due to the rotational symmetry of the system, the angular momentum is a good quantum number. The BdG solutions are then classified by the angular momentum. To keep the rotational symmetry, there is only the following combination of the order parameters for the C and U vortices:

$$\Delta_+(r,\phi)=\Delta_+(r)e^{i\phi},\quad \Delta_-(r,\phi)=\Delta_-(r)e^{i3\phi},\quad (C\ \text{vortex}), \tag{6a}$$

$$\Delta_+(r,\phi)=\Delta_+(r)e^{-i\phi},\quad \Delta_-(r,\phi)=\Delta_-(r)e^{i\phi},\quad (U\ \text{vortex}), \tag{6b}$$

where Δ_+ and Δ_- are the dominant and admixed components, respectively. Hence the wave function u_n couples with v_n in the following angular momentum spaces:[17]

$$u_n^l\leftrightarrow v_n^{l-2}\quad (C\ \text{vortex}), \tag{7}$$

$$u_n^l\leftrightarrow v_n^l\quad (U\ \text{vortex}), \tag{8}$$

where the superscripts represent the angular momenta of u_n and v_n. The Ginzburg-Landau (GL) calculation showed that the U vortex is energetically favored.[21] However, in a real sample we can expect two types $(p_x\pm ip_y)$ of domains, so that there are both C and U vortices in the presence of an external magnetic field. We solve the two-dimensional single-vortex problem on a disk of radius R. Since we treat a cylindrical system, it is convenient to expand wave functions by the following base functions:

$$\begin{pmatrix}u_n(\boldsymbol{r})\\ v_n(\boldsymbol{r})\end{pmatrix}=\sum_j\begin{pmatrix}u_{lnj}e^{il\phi}\varphi_{lj}(r)\\ v_{l'nj}e^{il'\phi}\varphi_{l'j}(r)\end{pmatrix}, \tag{9a}$$

$$\varphi_{lj}(r)=\frac{1}{\sqrt{\pi R^2}}J_l\left(\frac{Z_{lj}r}{R}\right). \tag{9b}$$

Here J_l is the lth Bessel function, Z_{lj} is the jth zero of J_l, and R is the radius of the system. l' in Eq. (9a) takes $l-2$ (l) for the C vortex (U vortex).

In a practical numerical calculation, we use no-dimensional quantities. We express them with bars as follows:

$$\nabla=\frac{1}{\xi_0}\bar{\nabla},\quad T=\Delta_0\bar{T},$$

$$\Delta_\pm=\Delta_0\bar{\Delta}_\pm,\quad E_n=\Delta_0\bar{E}_n,$$

$$\mu=\Delta_0\bar{\mu},\quad E_c=\Delta_0\bar{E}_c,$$

$$\boldsymbol{r}=\xi_0\bar{\boldsymbol{r}},\quad \Box_\pm=\frac{1}{\xi_0}\bar{\Box}_\pm,$$

$$u_n=\frac{1}{\xi_0}\bar{u}_n,\quad v_n=\frac{1}{\xi_0}\bar{v}_n,$$

$$eA_0=\Delta_0\bar{a}_0,\quad \frac{e}{c}\boldsymbol{A}=\frac{1}{\xi_0}\bar{\boldsymbol{a}},$$

$$n=\frac{1}{\xi_0^2}\bar{n},\quad n_0=\frac{1}{\xi_0^2}\bar{n}_0,$$

$$\boldsymbol{J}=\frac{e}{m\xi_0^3}\bar{\boldsymbol{J}}.$$

Here Δ_0 (unit of energy) is the magnitude of the order parameter at $T=0$. $\xi_0=v_F/\Delta_0$ (unit of length) is the superconducting coherence length. Using these nondimensional quantities, we obtain the following set of equations:

$$\bar{h}_0\bar{u}_n-\frac{i}{k_F\xi_0}\sum_\pm\left[\bar{\Delta}_\pm\bar{\Box}_\pm+\frac{1}{2}(\bar{\Box}_\pm\bar{\Delta}_\pm)\right]\bar{v}_n=\bar{E}_n\bar{u}_n, \tag{10a}$$

$$-\bar{h}_0^*\bar{v}_n-\frac{i}{k_F\xi_0}\sum_\pm\left[\bar{\Delta}_\pm\bar{\Box}_\pm+\frac{1}{2}(\bar{\Box}_\pm\bar{\Delta}_\pm)\right]^*\bar{u}_n=\bar{E}_n\bar{v}_n, \tag{10b}$$

$$\bar{h}_0=\frac{1}{2k_F\xi_0}(-i\bar{\nabla}+\bar{\boldsymbol{a}})^2-\bar{a}_0-\bar{\mu}, \tag{10c}$$

$$\bar{\Delta}_\pm(\bar{\boldsymbol{r}})=-ig\frac{1}{2k_F\xi_0}\sum_{0\le\bar{E}_n\le\bar{E}_c}\tanh\left(\frac{\bar{E}_n}{2\bar{T}}\right)[\bar{v}_n^*(\bar{\boldsymbol{r}})\bar{\Box}_\pm\bar{u}_n(\bar{\boldsymbol{r}})-\bar{u}_n(\bar{\boldsymbol{r}})\bar{\Box}_\mp\bar{v}_n^*(\bar{\boldsymbol{r}})], \tag{10d}$$

$$\bar{n}(\bar{\boldsymbol{r}})=2\sum_{\bar{E}_n}|\bar{u}_n(\bar{\boldsymbol{r}})|^2f(\bar{E}_n), \tag{10e}$$

$$\bar{\boldsymbol{J}}(\bar{\boldsymbol{r}})=-i\sum_{\bar{E}_n}[\bar{u}_n^*(\bar{\boldsymbol{r}})\bar{\nabla}\bar{u}_n(\bar{\boldsymbol{r}})-\bar{u}_n(\bar{\boldsymbol{r}})\bar{\nabla}\bar{u}_n^*(\bar{\boldsymbol{r}})]f(\bar{E}_n)-\bar{n}(\bar{\boldsymbol{r}})\bar{\boldsymbol{A}}(\bar{\boldsymbol{r}}), \tag{10f}$$

$$\bar{\nabla}^2\bar{a}_0(\bar{\boldsymbol{r}})=-\frac{\pi}{k_F\xi_0}\left(\frac{\xi_0}{\lambda_{\mathrm{TF}}}\right)^2[\bar{n}_0-\bar{n}(\bar{\boldsymbol{r}})], \tag{10g}$$

$$\bar{\nabla}^2\bar{\boldsymbol{a}}(\bar{\boldsymbol{r}})=-\left(\frac{\xi_0}{\lambda_L}\right)^2\frac{1}{\bar{n}_0}\bar{\boldsymbol{J}}(\bar{\boldsymbol{r}}). \tag{10h}$$

Here λ_{TF} and λ_L are the Thomas-Fermi screening length and London penetration depth, respectively. They are given by

$$\lambda_{\mathrm{TF}}^2=\frac{1}{4\pi e^2N(0)}=\frac{d}{4e^2m}, \tag{11a}$$

$$\lambda_L^2=\frac{c^2}{4\pi}\frac{md}{e^2n_0}, \tag{11b}$$

where $N(0)$ is the density of states at Fermi energy. For a two-dimensional layer system, it is given by $N(0)=m/\pi d$. g in Eq. (10d) is a nondimensional coupling for the p-wave defined as $g=V_p\Omega/(\Delta_0\xi_0^2)$. We have three no-dimensional parameters: $k_F\xi_0$, $\lambda_{\mathrm{TF}}/\xi_0$, and λ_L/ξ_0.

In our numerical calculation, we obtain $\bar{\Delta}_\pm(\bar{\boldsymbol{r}})$, $\bar{a}_0(\bar{\boldsymbol{r}})$, and $\bar{\boldsymbol{a}}(\bar{\boldsymbol{r}})$ by solving Eq. (10) iteratively within a Gygi-Schlüter method.[22] In the self-consistent calculation we fix the total number of electrons to the normal state value by adjusting $\bar{\mu}$.

III. NUMERICAL RESULTS

Let us discuss our BdG self-consistent solutions. First we show the order parameters in Fig. 1(a). The admixed component Δ_- is induced around the vortex core as expected. It shows the asymptotic behavior $\Delta_-\propto r$ ($\Delta_-\propto r^3$) for the U vortex (C vortex), which is consistent with the GL result.[21] $|\Delta_-|$ for the U vortex is larger than for the C vortex. This indicates that the U vortex gains much condensation energy. In Fig. 1(b) we show several energy eigenvalues of the BdG equation. We note that both vortices have zero-energy bound states.[23] The appearance of the zero-energy states is a consequence of the symmetric property of the BdG equation [Eq. (2)]. As we discuss below, the bound state for $l_u=0$ is very important to the vortex charging effect,[15,24] where l_u is the angular momentum of the wave function u_n. B_C and B_U in Fig. 1(b) represent the bound state. Next we show the charge density around the vortex core. As in Fig. 2(a), a large charge density appears in the vortex core.[24] The induced electric field is screened as we go far from the vortex center. Figure 2(b) is the spatial dependence of the electron density at various temperatures. At $T=0$ the electron density is suddenly decreased in the core region, which results in a vortex charge. With an increase of temperature, the electron density becomes uniform and the charge density is reduced accordingly. Contrary to the C vortex, the electron density is almost uniform at all temperatures for the U vortex, so that the vortex charge is very small in this case.

Let us explain the microscopic origin of the vortex charging effect. First we discuss the C vortex case. There are two contributions to the electron density n. One is from bound states, and the other is from extended states. We call the former n_B, and the latter n_E ($n=n_B+n_E$). In general only $l_u=0$ states contribute to the local electron density at the vortex center. In a microscopic study we find the important

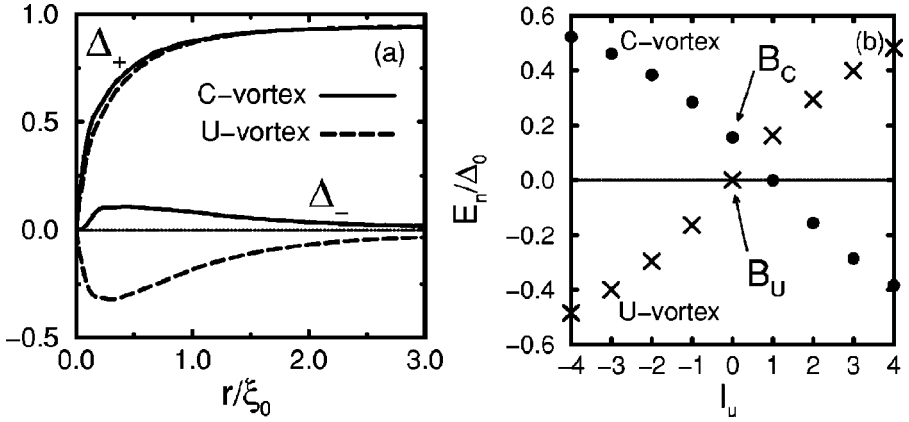

FIG. 1. Self-consistent results at $T=0$. (a) Order parameters scaled by Δ_0, which is the order parameter at $T=0$ in the bulk region. $\xi_0=v_F/\Delta_0$ is the coherence length. The set of parameters is taken as $R=8\xi_0$, $k_F\xi_0=16$, $\lambda_L=\xi_0$, $\lambda_{TF}=1/k_F$, and $E_c=\mu$. Here λ_L and λ_{TF} are the London and Thomas-Fermi screening lengths, respectively. (b) Bound-state energy spectrum for the C vortex (circle) and the U vortex (X). l_u is the angular momentum of the wave function u_n. The bound states represented by B_C and B_U are important in the vortex charging effect (see the text). Extended states lie continuously in a $|E_n|\geqslant\Delta_0$ region.[17]

role of the bound state with zero angular momentum ($l_u=0$).[15,24] At zero temperature only the $E_n\leqslant 0$ states are effective in Eq. (3). Therefore, the bound state B_C in Fig. 1(b) cannot contribute to the electron density, since this state is unoccupied [Fig. 3(a)]. n_B is then suddenly decreased in the core region as in Fig. 3(b), and the total electron density is decreased close to the vortex center, resulting in a finite vortex charge. At finite temperatures the contribution from the B_C state comes out [Fig. 3(a)] due to the finite Fermi distribution function in Eq. (3) for $E_n>0$. Correspondingly, n_B increases in the core region as shown in Fig. 3(b). At $T=0.3\Delta_0$, which is larger than the energy of B_C, the electron density is almost uniform due to the contribution from the B_C state. The vortex charge is then reduced strongly at high temperatures, as shown in Fig. 2(b).

Next we discuss the U vortex. Contrary to the C vortex, the B_U bound state in Fig. 1(b) can contribute to the electron density at all temperatures, since this state is located at zero energy. As a consequence, the electron density for the U vortex is almost uniform. In the U vortex case we find a very small temperature dependence in the electron density, since the B_U state is located at zero energy and participates in energy excitations with the same rate at all temperatures. We note that the electron density for the U vortex is very similar to that for the C vortex at $T=0.3\Delta_0$, where the B_C state is occupied. We conclude that the appearance of the vortex charge depends on the position of the $l_u=0$ bound state relative to the temperature. In the conventional s-wave case, the vortex charge always appears at sufficiently low temperatures,[15] which is similar to the C vortex result.

Let us mention the effect of charge screening. We show the total electron density n and the contribution from extended states n_E for two cases, where charge screening is taken into account or not (see Fig. 4). In the no-charge-screening case, the contribution from extended states n_E is small at the vortex core. The total electron density n is then decreased, resulting in a larger vortex charge. Note that the scalar potential in Eq. (10g) is zero ($\overline{a_0}=0$) for no charge

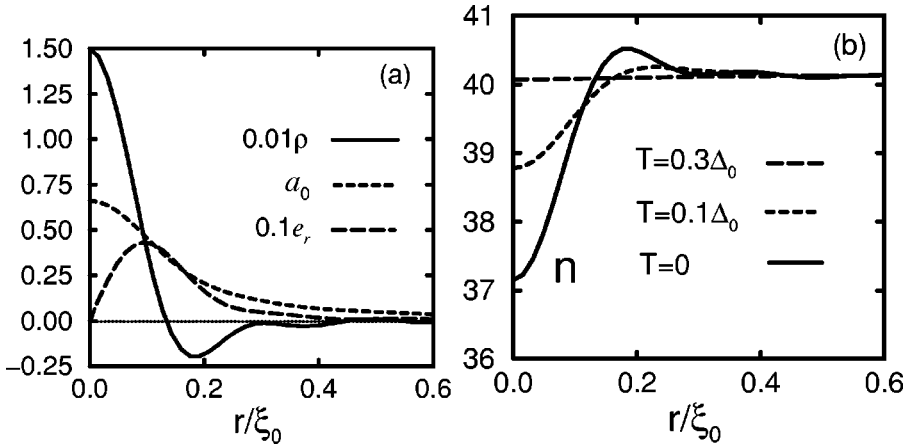

FIG. 2. (a) Dimensionless scalar potential $a_0=eA_0/\Delta_0$, electric field $e_r=-\xi_0\partial_r a_0$, and charge density $\rho=\xi_0(1/r+\partial_r)e_r$ for the C vortex at $T=0$. (b) Spatial dependence of the electron density n in $1/\xi_0^2$ units at various temperatures. The charge density is given by $\rho(r)=e[n(\infty)-n(r)]$.

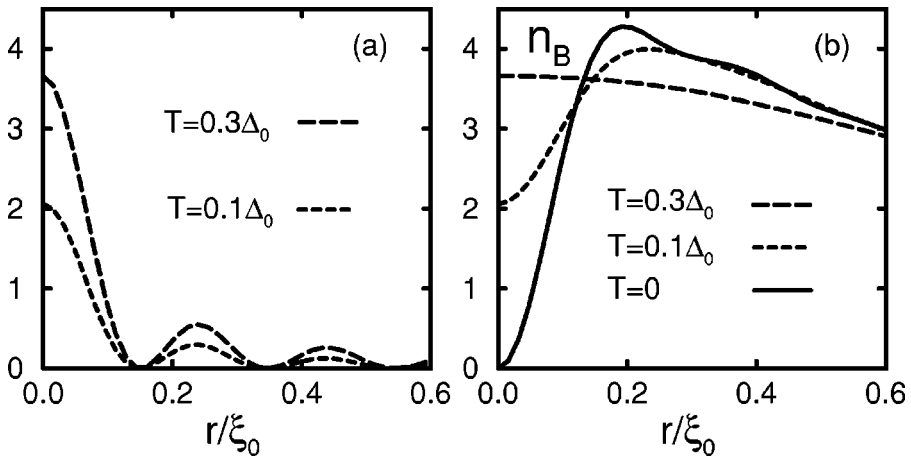

FIG. 3. Local electron density for the C vortex in $1/\xi_0^2$ units. (a) Contribution from the bound state B_C [Fig. 1(b)]. It is zero at $T=0$. (b) Bound-state contribution n_B.

screening ($\lambda_{\mathrm{TF}}\rightarrow\infty$). Therefore, the scalar potential does not work to screen the vortex charge. On the other hand, when the charge screening turns on, quasiparticles respond to the vortex charge via the scalar potential $\bar{a}_0$ in the BdG equations (10a)–(10c). n_E is then increased to cancel the vortex charge. In contrast to the extended state, the electron density of the bound states n_B does not exhibit a difference between the charge screening and no screening cases. Since the bound states are localized around the vortex core, their wave functions hardly modulate, while the extended states do easily. Hence the extended states quickly respond to the electric field, and they screen the vortex charge. However, there still remains a substantial vortex charge.

We discuss the effect of a magnetic field. The Chern-Simons physics[16] and the Bernoulli effect[25] take place in the presence of a magnetic field. To see this effect we compare the two results, where $\bar{\boldsymbol{a}}$ is present or ignored (no magnetic field). The scalar potential $\bar{a}_0$ is taken into account in both cases. Our result shows that the effect of the magnetic field is too small to be seen. Thus we find that the vortex charge is mainly determined by the microscopic quasiparticle structure, which reflects the phase winding of the chiral pairing. Figure 5 shows a schematic picture of the energy spectrum of vortex bound states for various winding pairings. The lowest-lying state appears at symmetric positions of l_u and l_v due to relation (2), where l_u and l_v are the angular momenta of u_n and v_n, respectively. For the C vortex the bound-state energy is positive for $l_u=0$, while it is negative or zero for the U vortex. Therefore, the C vortex is always charged up at low temperatures, while the U vortex is not. Thus the vortex charge can be discussed in terms of the vortex bound states for all types of chiral pairings. Similarly, we can understand that the s-wave (zero winding) vortex is charged up.[15]

Finally let us discuss nonchiral pairings, such as p_x, p_y, and $d_{x^2-y^2}$-waves. These states are all gapless, and it was

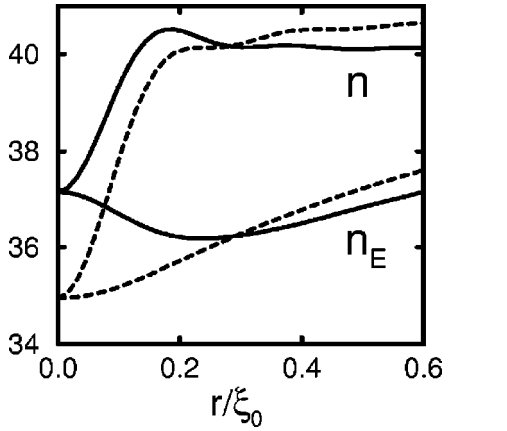

FIG. 4. Total electron density n and contribution from the extended states n_{E} at $T=0$. Solid lines represent the result with charge screening ($\lambda_{\mathrm{TF}}=1/k_F$), while dashed lines are the result without charge screening ($\lambda_{\mathrm{TF}}\rightarrow\infty$).

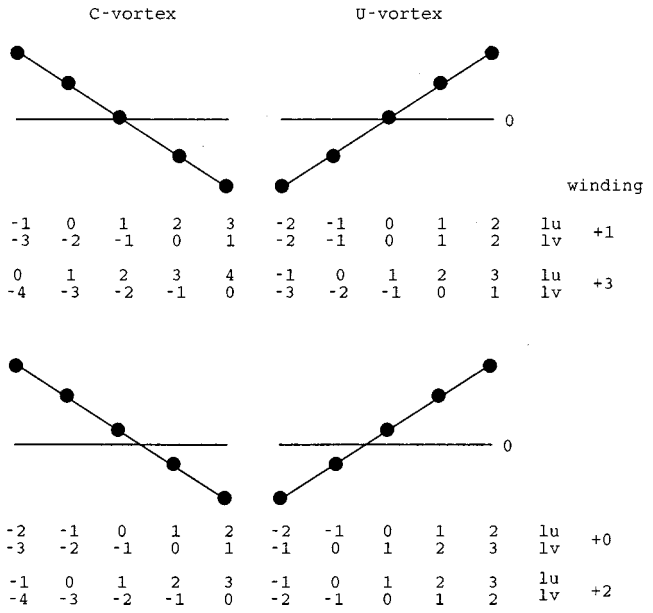

FIG. 5. Schematic picture of bound-state energy spectrum for various winding pairings. Numbers represent the angular momenta of u_n and v_n (l_u and l_v).

reported that there is no bound states for the $d_{x^2-y^2}$-wave.[26] Since the system is anisotropic in this case, the energy eigenstates are not classified by the angular momentum. Therefore the above argument for the vortex charging is difficult to apply to this case. However, our result implies that the detailed quasiparticle structure in the vortex core is important for the vortex charging effect even in the gapless pairing cases.

IV. SUMMARY AND DISCUSSIONS

In conclusion, we have solved the problem of a single $p_x \pm ip_y$-wave vortex self-consistently within the Bogoliubov–de Gennes theory. The full self-consistent calculation, including both charge and current screenings, was performed to investigate vortex problems. Due to the time-reversal symmetry breaking, there are two types of vortices. We found a substantial vortex charge in the *C*-vortex case, while the vortex charge is suppressed for *U*-vortex case. We conclude that the vortex charging effects are mainly determined by the local quasiparticle structure around the vortex core, reflecting the chiral $p_x \pm ip_y$-wave pairing. Especially the lowest vortex bound state is very important for the charging effect at low temperatures.

In a real sample we can expect two types ($p_x \pm ip_y$) of domains. Therefore, we expect both *C* and *U* vortices in the presence of an external magnetic field. In domains, where the *C* vortex is realized, an electronic field is induced due to the vortex charge. Therefore, the charge of the *C* vortex can be detected. If we use a field-cooled sample, a single domain forming a *U* vortex is realized all over the sample, since the *U* vortex is energetically favorable.[21] In this case it is difficult to find a signal from the *U* vortex, since the charge of the *U* vortex is much smaller than that of the *C* vortex. Thus we can distinguish between *C* and *U* vortices.

How can we detect the vortex charge? The vortex charge can induce a lattice distortion, and it scatters neutrons. It was reported that a polarized neutron scattering can be used to detect the vortex charge.[27] The NQR is also one of the possible experiments which can detect the vortex charging effect, since the NQR detects the local electric field induced by the vortex charge. Very recently, Kumagai *et al.* reported that a vortex charge is observed by the NQR in a high-T_c material.[28] Thus a detection of the vortex charge is in progress now. It is very exciting if the vortex charge of the chiral superconductor is detected, since it can provide a very strong evidence of a *rotating* Cooper pair.

ACKNOWLEDGMENTS

The authors express their sincere thanks to M. Sigrist, G. Blatter, and A. Furusaki for many stimulating discussions. One of the authors (M.M.) thanks N. Hayashi for helpful discussions on the BdG equation and the vortex charging effect. He would like to acknowledge M. Koga for a critical reading of the manuscript. This work was supported by Casio Science Promotion Foundation.

APPENDIX A: DERIVATION OF BOGOLIUBOV–DE GENNES EQUATION AND GAP EQUATION

In this appendix we derive the Bogoliubov–de Gennes equation and gap equation for the p_x+ip_y-wave superconductor, which we use in the text. Let us start from the following Bogoliubov–de Gennes equations:

$$h_0(\boldsymbol{r})u_n(\boldsymbol{r})+\int d\boldsymbol{r}'\,\Delta(\boldsymbol{r},\boldsymbol{r}')v_n(\boldsymbol{r}')=E_n u_n(\boldsymbol{r}), \quad \text{(A1a)}$$

$$-h_0^*(\boldsymbol{r})v_n(\boldsymbol{r})-\int d\boldsymbol{r}'\,\Delta^*(\boldsymbol{r},\boldsymbol{r}')u_n(\boldsymbol{r}')=E_n v_n(\boldsymbol{r}). \quad \text{(A1b)}$$

Coordinates $\boldsymbol{r}$ and $\boldsymbol{r}'$ can be transformed into center-of-mass and relative coordinates:

$$\boldsymbol{R}=\frac{\boldsymbol{r}+\boldsymbol{r}'}{2}, \quad \boldsymbol{X}=\boldsymbol{r}-\boldsymbol{r}'. \quad \text{(A2)}$$

The p_x+ip_y-wave pairing is expressed as

$$\Delta(\boldsymbol{R},\boldsymbol{k})=\Delta_x(\boldsymbol{R})\frac{k_x}{k_F}+i\Delta_y(\boldsymbol{R})\frac{k_y}{k_F}, \quad \text{(A3a)}$$

$$\begin{aligned}\Delta(\boldsymbol{R},\boldsymbol{X})&=\frac{1}{(2\pi)^2}\int d\boldsymbol{k}e^{i\boldsymbol{k}\cdot\boldsymbol{X}}\Delta(\boldsymbol{R},\boldsymbol{k})\\&=i\frac{1}{(2\pi)^2}\int d\boldsymbol{k}\frac{1}{k_F}[\Delta_x(\boldsymbol{R})\partial_{x'}+i\Delta_y(\boldsymbol{R})\partial_{y'}]e^{i\boldsymbol{k}\cdot(\boldsymbol{r}-\boldsymbol{r}')}\\&=\frac{i}{k_F}[\Delta_x(\boldsymbol{R})\partial_{x'}+i\Delta_y(\boldsymbol{R})\partial_{y'}]\delta(\boldsymbol{r}-\boldsymbol{r}'). \quad \text{(A3b)}\end{aligned}$$

Here Δ_x and Δ_y are the p_x and p_y components of the order parameter. Substituting Eq. (A3b) into Eq. (A1), we obtain

$$h_0(\boldsymbol{r})u_n(\boldsymbol{r})-\frac{\mathrm{i}}{k_F}\Big\{\Delta_x(\boldsymbol{r})\partial_x+i\Delta_y(\boldsymbol{r})\partial_y+\frac{1}{2}[\partial_x\Delta_x(\boldsymbol{r})+i\partial_y\Delta_y(\boldsymbol{r})]\Big\}v_n(\boldsymbol{r})=E_n u_n(\boldsymbol{r}), \quad \text{(A4a)}$$

$$-h_0^*(\boldsymbol{r})v_n(\boldsymbol{r})-\frac{i}{k_F}\Big\{\Delta_x(\boldsymbol{r})\partial_x-i\Delta_y(\boldsymbol{r})\partial_y+\frac{1}{2}[\partial_x\Delta_x(\boldsymbol{r})-i\partial_y\Delta_y(\boldsymbol{r})]\Big\}u_n(\boldsymbol{r})=E_n v_n(\boldsymbol{r}). \quad \text{(A4b)}$$

Next we derive the gap equation. The order parameter is defined by

$$\begin{aligned}\Delta(\boldsymbol{r},\boldsymbol{r}')&=V(\boldsymbol{r},\boldsymbol{r}')\sum_{0\le E_n\le E_c}\tanh\left(\frac{E_n}{2T}\right)u_n(\boldsymbol{r}')v_n^*(\boldsymbol{r})\\&\equiv V(\boldsymbol{r},\boldsymbol{r}')D(\boldsymbol{r},\boldsymbol{r}'), \quad \text{(A5)}\end{aligned}$$

where E_c is a cutoff energy. For the *p*-wave pairing, we assume the following *p*-wave interaction:

$$V(\boldsymbol{r},\boldsymbol{r}')=-\frac{V_p\Omega}{(2\pi)^2}\int d\boldsymbol{k}e^{i\boldsymbol{k}\cdot\boldsymbol{X}}\frac{k^2}{k_F^2}. \tag{A6}$$

Here $V_p>0$ and Ω are the p-wave attractive interaction and the two-dimensional volume of the system, respectively. The order parameter is then expressed as

$$\Delta(\boldsymbol{R},\boldsymbol{k})=\int d\boldsymbol{X}e^{-i\boldsymbol{k}\cdot\boldsymbol{X}}\Delta(\boldsymbol{r},\boldsymbol{r}')=-V_p\Omega\int d\boldsymbol{k}'\frac{k'^2}{k_F^2}\frac{1}{(2\pi)^2}\times\int d\boldsymbol{X}e^{-i\boldsymbol{k}\cdot\boldsymbol{X}}D\left(\boldsymbol{R}+\frac{\boldsymbol{X}}{2},\boldsymbol{R}-\frac{\boldsymbol{X}}{2}\right)e^{i\boldsymbol{k}'\cdot\boldsymbol{X}}. \tag{A7}$$

We expand $D[\boldsymbol{R}+(\boldsymbol{X}/2),\boldsymbol{R}-(\boldsymbol{X}/2)]$ as

$$D\left(\boldsymbol{R}+\frac{\boldsymbol{X}}{2},\boldsymbol{R}-\frac{\boldsymbol{X}}{2}\right)\simeq R(\boldsymbol{R},\boldsymbol{R})+\left[\frac{\partial D(\boldsymbol{R},\boldsymbol{R}')}{\partial\boldsymbol{R}}-\frac{\partial D(\boldsymbol{R},\boldsymbol{R}')}{\partial\boldsymbol{R}'}\right]_{\boldsymbol{R}'\to\boldsymbol{R}}\cdot\frac{\boldsymbol{X}}{2}, \tag{A8}$$

and obtain

$$\Delta(\boldsymbol{R},\boldsymbol{k})\simeq-V_p\Omega\frac{k^2}{k_F^2}\sum_{0\leqslant E_n\leqslant E_c}\tanh\left(\frac{E_n}{2T}\right)u_n(\boldsymbol{R})v_n^*(\boldsymbol{R})-iV_p\Omega\frac{\boldsymbol{k}}{k_F^2}\cdot\left(\frac{\partial}{\partial\boldsymbol{R}}-\frac{\partial}{\partial\boldsymbol{R}'}\right)\sum_{0\leqslant E_n\leqslant E_c}\tanh\left(\frac{E_n}{2T}\right)\times u_n(\boldsymbol{R})v_n^*(\boldsymbol{R}')|_{\boldsymbol{R}'\to\boldsymbol{R}}. \tag{A9}$$

The first term in Eq. (A9) is zero due to the p-wave pairing. Since $\Delta(\boldsymbol{R},\boldsymbol{k})$ can be divided into two parts as in Eq. (A3a), the gap equation takes the following form:

$$\Delta_x(\boldsymbol{r})=-V_p\Omega\frac{i}{k_F}(\partial_x-\partial_{x'})\sum_{0\leqslant E_n\leqslant E_c}\tanh\left(\frac{E_n}{2T}\right)\times u_n(\boldsymbol{r})v_n^*(\boldsymbol{r}')|_{\boldsymbol{r}'\to\boldsymbol{r}}, \tag{A10a}$$

$$\Delta_y(\boldsymbol{r})=-V_p\Omega\frac{1}{k_F}(\partial_y-\partial_{y'})\sum_{0\leqslant E_n\leqslant E_c}\tanh\left(\frac{E_n}{2T}\right)\times u_n(\boldsymbol{r})v_n^*(\boldsymbol{r}')|_{\boldsymbol{r}'\to\boldsymbol{r}}. \tag{A10b}$$

For a cylindrical system, it is convenient to introduce the following form for order parameters:

$$\Delta_\pm(\boldsymbol{r})=\tfrac{1}{2}[\Delta_x(\boldsymbol{r})\pm\Delta_y(\boldsymbol{r})]. \tag{A11}$$

Here $\Delta_\pm$ is the order parameter for the $p_x\pm ip_y$-wave pairing. By using the $\Delta_\pm$ representation, the Bogoliubov–de Gennes equation and the gap equations are expressed as

$$h_0(\boldsymbol{r})u_n(\boldsymbol{r})-\frac{\mathrm{i}}{k_F}\left\{\Delta_+(\boldsymbol{r})\Box_++\Delta_-(\boldsymbol{r})\Box_-+\frac{1}{2}[\Box_+\Delta_+(\boldsymbol{r})+\Box_-\Delta_-(\boldsymbol{r})]\right\}v_n(\boldsymbol{r})=E_nu_n(\boldsymbol{r}), \tag{A12a}$$

$$-h_0^*(\boldsymbol{r})v_n(\boldsymbol{r})-\frac{i}{k_F}\left\{\Delta_+(\boldsymbol{r})\Box_++\Delta_-(\boldsymbol{r})\Box_-+\frac{1}{2}[\Box_+\Delta_+(\boldsymbol{r})+\Box_-\Delta_-(\boldsymbol{r})]\right\}^*u_n(\boldsymbol{r})=E_nv_n(\boldsymbol{r}), \tag{A12b}$$

$$\Delta_\pm(\boldsymbol{r})=-V_p\Omega\frac{i}{2k_F}(\Box_\mp-\Box'_\mp)\sum_{0\leqslant E_n\leqslant E_c}\tanh\left(\frac{E_n}{2T}\right)\times u_n(\boldsymbol{r})v_n^*(\boldsymbol{r}')|_{\boldsymbol{r}'\to\boldsymbol{r}}, \tag{A12c}$$

$$\Box_\pm=\partial_x\pm i\partial_y. \tag{A12d}$$

[1] Y. Maeno, H. Hashimoto, K. Yoshida, S. Nishizaki, T. Fujita, J. G. Bednorz, and F. Lichtenberg, Nature (London) **372**, 532 (1994).

[2] K. Ishida, Y. Kitaoka, K. Asayama, S. Ikeda, S. Nishizaki, Y. Maeno, K. Yoshida, and T. Fujita, Phys. Rev. B **56**, R505 (1997).

[3] A. P. Mackenzie, R. K. W. Haselwimmer, A. W. Tyler, G. G. Lonzarich, Y. Mori, S. Nishizaki, and Y. Maeno, Phys. Rev. Lett. **80**, 161 (1998).

[4] G. M. Luke, Y. Fudamoto, K. M. Kojima, M. I. Larkin, J. Merrin, B. Nachumi, Y. J. Uemura, Y. Maeno, Z. Q. Mao, Y. Mori, H. Nakamura, and M. Sigrist, Nature (London) **394**, 558 (1998).

[5] K. Ishida, H. Mukuda, Y. Kitaoka, K. Asayama, Z. Q. Mao, Y. Mori, and Y. Maeno, Nature (London) **396**, 658 (1998).

[6] M. Sigrist, D. F. Agterberg, A. Furusaki, C. Honerkamp, K. K. Bg, T. M. Rice, and M. E. Zhitomirsky, Physica (Amsterdam) **317C-318C**, 134 (1999).

[7] Y. Yoshida, A. Mukai, R. Settai, K. Miyake, Y. Inada, Y. Onuki, K. Betsuyaku, H. Harima, T. D. Matsuda, Y. Aoki, and H. Sato, J. Phys. Soc. Jpn. **68**, 3041 (1999).

[8] S. NishiZaki, Y. Maeno, and Z. Q. Mao, J. Phys. Soc. Jpn. **69**, 572 (2000).

[9] K. Ishida, H. Mukuda, Y. Kitaoka, Z. Q. Mao, Y. Mori, and Y. Maeno, Phys. Rev. Lett. **84**, 5387 (2000).

[10] D. F. Agterberg, T. M. Rice, and M. Sigrist, Phys. Rev. Lett. **78**, 3374 (1997).

[11] K. Miyake and O. Narikiyo, Phys. Rev. Lett. **83**, 1423 (1999).

[12] Y. Hasegawa, K. Machida, and M. Ozaki, J. Phys. Soc. Jpn. **69**, 336 (2000).

[13] D. I. Khomskii and A. Freimuth, Phys. Rev. Lett. **75**, 1384 (1995).

[14] G. Blatter, M. Feigel'man, V. Geshkenbein, A. Larkin, and A. Otterlo, Phys. Rev. Lett. **77**, 566 (1996).

[15] N. Hayashi, M. Ichioka, and K. Machida, J. Phys. Soc. Jpn. **67**, 3368 (1998).

[16] J. Goryo, Phys. Rev. B **61**, 4222 (2000).

[17] M. Matsumoto and M. Sigrist, J. Phys. Soc. Jpn. **68**, 724 (1999).

[18] R. Heeb, Doctor thesis, ETH Zürich (2000).

[19] A. Furusaki, M. Matsumoto, and M. Sigrist, Phys. Rev. B **64**, 054514 (2001).

[20] D. F. Agterberg, Phys. Rev. Lett. **80**, 5184 (1998); Phys. Rev. B **58**, 14484 (1998).
[21] R. Heeb and D. F. Agterberg, Phys. Rev. B **59**, 7076 (1999).
[22] F. Gygi and M. Schlüter, Phys. Rev. B **43**, 7609 (1991).
[23] G. E. Volovik, Pis'ma Zh. Éksp. Teor. Fiz. **70**, 601 (1999) [JETP Lett. **70**, 609 (1999)].
[24] M. Matsumoto and M. Sigrist, Physica B **281&282**, 973 (2000).
[25] Yu. M. Ivanchenko and A. N. Omel'yanchuk, Fiz. Nizk. Temp. **11**, 889 (1985) [Sov. J. Low Temp. Phys. **11**, 490 (1985)].
[26] M. Franz and Z. Tešanović, Phys. Rev. Lett. **80**, 4763 (1998).
[27] K. U. Neumann, F. Kusmartsev, H.-J. Lauter, O. Schärpf, T. J. Smith, and K. R. A. Ziebeck, Eur. Phys. J. B **1**, 5 (1998).
[28] K. Kumagai, K. Nozaki, and Y. Matsuda, Phys. Rev. B **63**, 144502 (2001).